INTERNATIONAL JOURNAL OF AUTOMOTIVE AND MECHANICAL ENGINEERING (IJAME)
ISSN: 2229-8649 e-ISSN: 2180-1606
VOL. 18, ISSUE 4, 9220 – 9229
DOI: https://doi.org/10.15282/ijame.18.4.2021.06.0709

ORIGINAL ARTICLE

Assessment of Partially Premixed Flame by In-Situ Adaptive Reduced Mechanisms in OpenFOAM

P. Kamma[1,2] and C. Suvanjumrat[1,2,*]

[1]Department of Mechanical Engineering, Faculty of Engineering, Mahidol University, Nakhon Pathom 73170, Thailand
[2]Laboratory of Computer Mechanics for Design (LCMD), Department of Mechanical Engineering, Faculty of Engineering, Mahidol University, Nakhon Pathom 73170, Thailand

ABSTRACT – The partially premixed flame was modelled using an open-source software based on finite volume method (FVM) of computational fluid dynamics (CFD), called OpenFOAM. The assessment of the tabulation dynamics adaptive chemistry (TDAC) algorithms for facilitating the computation was of interest. A total of seven models were performed, consisting of six models of the TDAC framework application and a direct computation model without TDAC. Simulation results were validated by comparing against the thermal flame height (HT) of Irandoost et al. [28]. The heat released rate was established from simulation results to identify the flame front and HT. This is a novel technique to illustrate the flame front, which agreed well with the experiment. Subsequently, it was found that all but one of the reduced mechanism methods agreed well in predicting the HT. The exception was DRGEP. Particularly, the CFD results were optimal. It was discovered that the TDAC based on the mechanism reduction called element flux analysis (EFA) was the second-fastest but optimal choice to solve the partially premixed flame model.

ARTICLE HISTORY
Received: 18th May 2021
Revised: 12th Sept 2021
Accepted: 3rd Dec 2021

KEYWORDS
CFD;
Flame;
Reacting flow;
Reduced mechanism;
TDAC

NOMENCLATURE

CFD	computational fluid dynamics
DAC	dynamics adaptive chemistry
DRG	direct relation graph
DRGEP	direct relation graph with error propagation
EFA	element flux analysis
HRR	heat released rate
HT	thermal flame height
ISAT	in situ adaptive chemistry
ODE	ordinary differential equation
PFA	path flux analysis
SA	sensitivity analysis
TDAC	tabulation dynamics chemistry

INTRODUCTION

Premixed combustion operates in the environmental air in which the air participates in the combustion process, called partially premixed combustion. Typical combustion finds in familiar domestic and industrial appliances. There is a challenging topic to deeply understand the combustion process for developing combustion equipment [1]. Computational fluid dynamics (CFD) is recent an excellent tool for investigating experiments instead. It manipulates the numerical approach to solve a set of Navier-Stokes equations together with the detailed chemistry. It allows that the user can access what happens during combustion progress. Therefore, combustion modelling carries out by supplementing the reaction mechanisms into the CFD model. It is a series of elementary reaction steps for detailing chemical activities involving ten to a hundred for species and a hundred to a thousand for reactions in only a simple hydrocarbon fuel [2]. It causes the size of the reaction mechanism to be a tremendous computational cost, which is difficult to obtain CFD results [3].

The computational cost mainly dominates combustion modelling by considering the detailed chemistry is evaluation of diffusion process and Jacobian operation. Diffusion is an integral process in inhomogeneous flow. It can use the mixture-averaged and multicomponent diffusion models to represent [4, 5]. The binary diffusion coefficient is the main cost in the mixture-averaged model that can scale up quadratically with the number of species. The multicomponent model can expand to three times of computational cost with numbers of species. Therefore, it is hard to accomplish the combustion simulation easily with large species numbers, although it can yield the most accurate and reliable results. Another numerically time-consuming known as the Jacobian operation involves an implicit integration solver [6]. It can

*CORRESPONDING AUTHOR | C. Suvanjumrat | ✉ chakrit.suv@mahidol.ac.th

amplify the cost in large-scale combustion due to the number of species and reactions. The Jacobian must reevaluate when any species are perturbed.

Numerical computation of combustion prefers to simplify the dimension of the model more than the detailed diffusion or the Jacobian operation reduction because it can implicitly diminish those computational costs [7, 8]. The efficient approach of reduced mechanisms is a representative subset of its original mechanism that selects only a few species and reactions. Reduction based on path analysis is an extensively studied activity. The conventional method is the graph-based method called the directed relation graph (DRG) [9]. The unimportant species also reactions are searched and eliminated by considering the degree of coupling via the digraph. Other reduced mechanisms can carry out by the reduction method based on DRG, such as DRG with error propagating (DRGEP) [10], DRG aided sensitivity (DRGASA) [11], path flux analysis (PFA) [12], and element flux analysis (EFA) [13]. The reduction based on the lumping technique is effective in grouping the correlated species [14]. The duplicated reactions, which are generated in species lumping, can further diminish. In addition, it is effective in hydrocarbon fuel that involves copious isomers, the same thermal existing, and transport attributes. The analytical time scale can conduct to dimensional detraction. The very-fast depleting species and fast reversible reaction can suppress by the traditional quasi-steady-state assumption (QSSA) [15] and partial equilibrium assumption (PEA) [16]. The differential equation is simplified to be algebraic that results in computing time-saving. To identify the QSS species and PE reaction, both QSSA and PEA require supplemental methods such as the computational singular perturbation (CSP) [17] and an intrinsic low-dimension manifold (ILDM) [18]. Moreover, the other conventional methods consisting of sensitivity analysis (SA) [19], artificial neural network [20], genetic algorithm, and eigenanalysis have a primary role involving the previous mentions.

An interesting technique is the extensive mechanism reduction is called the tabulation dynamic adaptive chemistry (TDAC) [21-23]. It is a combined version of in-situ adaptive chemistry (ISAT) [24] and the reduction method based on path analysis to be a runtime reduction. The advantage is, no need for the pre-processing of a reduced mechanism. Remarkably, the pre-processing can assure only global comprehensiveness by specifying a pre-threshold value, which agrees with the desired error limit at any sample point. Some species can be missing in any circumstances locally. This point is particularly relevant in the state of an inhomogeneous. In addition, this also is in a wide range of thermochemical conditions. Also, many works of literature offer a good compromise in a particular combustor. There exists, however, rarely literature adopting TDAC to partially premixed combustion.

Because surrounding air continuously entrant to the combustion zone causes variation in reaction conditions, this research aims to utilise TDAC to model the partially premixed flame. It is carried out by the free license CFD toolbox based on a finite volume method (FVM) called OpenFOAM [25, 26]. A detailed reaction mechanism (GRI-Mech 3.0, [27]) developed for natural fuel combustion is employed to perform the reduction. There are seven cases of combustion modelling comprising one model without applying reduction technique, one facilitated model by ISAT, and five models by TDAC. The results were validated against the measurement of thermal flame height. Six cases (one ISAT and five TDACs) were examined to obtain the best promising method. It can reach an insight into complex combustion phenomenon with accuracy and compact computational cost instead of the existing traditional modelling and experiment.

GOVERNING EQUATIONS

The CFD partially premixed flame modelling performs to solve a set of conservative flow equations. These are in the laminar flow comprising the mass, momentum, species mass fraction, and energy follow Eq. (1) to Eq. (4), respectively.

$$\frac{\partial \rho}{\partial t} + \frac{\partial \rho u_i}{\partial x_i} = 0 \tag{1}$$

$$\frac{\partial \rho u_i}{\partial t} + \frac{\partial \rho u_i u_j}{\partial x_i} = \frac{\partial p}{\partial x_i} + \frac{\partial \tau_{ij}}{\partial x_i} + F_i \tag{2}$$

$$\frac{\partial \rho Y_k}{\partial t} + \frac{\partial \rho u_i Y_k}{\partial x_i} = \frac{\partial}{\partial x_i}\left(\mu \frac{\partial Y_k}{\partial x_i}\right) + \dot{\omega}_k \tag{3}$$

$$\frac{\partial}{\partial t}(\rho h_s) + \frac{\partial}{\partial x_i}(\rho u_i h_s) = \frac{\partial}{\partial x_i}\left(k \frac{\partial T}{\partial x_i}\right) - \frac{\partial}{\partial x_i}\left(\sum_{k=1}^{N} h_k \left(\frac{\mu}{\rho}\left(\frac{\partial Y_k}{\partial x_i}\right)\right)\right) + \dot{Q} + S_i \tag{4}$$

where ρ is the gaseous density, u is velocity, p is pressure, τ_{ij} is the viscous stress tensor, F is the body force, Y is the mass fraction of species, μ is the dynamic viscosity, $\dot{\omega}$ is the reaction rate, h is the sensible enthalpy, k is the thermal conductivity, h_k is the enthalpy of species k, $\dot{Q}$ is the heat released due to chemical reaction, and S is the energy source term due to thermal radiation.

IMPLEMENTATION

Computational Facilitation

The TDAC frameworks use both the ISAT algorithm and the reduction mechanism method are layering between flow and stiff ODE of chemistry solver shown in Figure 1. The ISAT algorithm, the first added layer in the TDAC framework, is used to store and manipulate the thermochemical composition data by the binary tree. The leaves of the binary tree store thermochemical composition, ψ^0, reaction mapping, $R(\psi^0)$, modified mapping gradient matrix A and description of the ellipsoid of accuracy. The node stores the hyperplane allowing ISAT to search throughout the binary tree to retrieve the required runtime data. As the first step of the TDAC, the CFD solver sends the queried thermochemical composition ψ^q into ISAT. It tries to calculate the reaction mapping for retrieving the stored value of previous time steps results. A linear interpolation computes the result, which has to validate in the ellipsoid of the accuracy region. The expression of linear interpolation mapping and ellipsoid of accuracy write as Eq. (5) and Eq. (6).

$$R^l(\psi^q) = R(\psi^0) + A(\psi^0)\left(\psi^q_{active} - \psi^0\right) \cong R(\psi^q) \tag{5}$$

$$R^l(\psi^q) = \delta\psi^T \left[\frac{\tilde{A}^T B^T B \tilde{A}}{\varepsilon^2_{ISAT}}\right]\left[\frac{\tilde{A}^T B^T B \tilde{A}}{\varepsilon^2_{ISAT}}\right]^T \delta\psi \leq 1 \tag{6}$$

where $\tilde{A}$ is the modified mapping gradient matrix, B is the scaling matrix, and ε_{ISAT} is the user-specified tolerance.

If the retrieval is impossible, it is unnecessary to solve the entire set of reaction mechanisms. So, the ψ^q is reduced to an active set of thermochemical composition ψ^q_{active} by a second added layer of reduction mechanism method. Next, active reaction mapping $R\left(\psi^q_{active}\right)$ is solved by the stiff ODE solver. During the calculation, ISAT will calculate the local error ε_{local}. It is compared with ε_{ISAT} to modify the binary tree by adding or growing. The ε_{local} is given as Eq. (7). The $R\left(\psi^q_{active}\right)$ is built up to $R(\psi^q)$ full in composition space and stored for subsequent use.

$$\varepsilon_{local} = R(\psi^q) - R^t(\psi^q) \leq \varepsilon_{ISAT} \tag{7}$$

The TDAC framework modifies the reduction mechanism method as a runtime reduction instead of pre-processing. The species and reactions will estimate in order of importance. Unimportant ones are disabled. The concentration of species as ψ^q_{active} was integrated by a stiff ODE solver using the implicit method. The result then returns to the CFD solver. The unimportant, the disabled species, with zero mass fractions, are not calculated and used while non-zero ones have only participated in the CFD solver. The reduced mechanism method used in this works is the reaction path analysis, including the directed relation graph (DRG), DRG with error propagation (DRGEP), path flux analysis (PFA), dynamic adaptive chemistry (DAC), and element flux analysis (EFA). A short description of these is given below.

The reduction based on reaction path analysis contains three steps used in analysing the various species. First, the degree of coupling between two species, called the path strength, r_{AB}, is computed. Next, the important species, such as reactants, important radicals, and productions, are searched by the initial and search-initiating species. The species with r_{AB} were compared to the user-defined threshold ε_{user} in which $r_{AB} < \varepsilon_{user}$ is disabled. The different values of r_{AB} resulting from each method achieve. Then the r_{AB} of DRG is the normalised contribution of species B to the net production rate of species A and is given by Eq. (8).

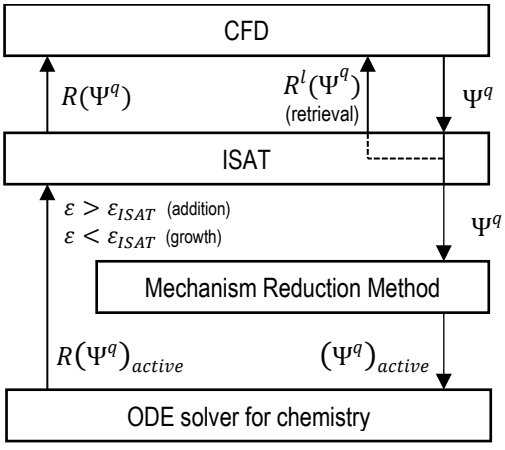

Figure 1. Schematic of TDAC framework.

$$r_{AB}^{DRG} = \frac{\sum_{i=1}^{N_r} |v_{A,i}\omega_i\delta_{B,i}|}{\sum_{i=1}^{N_r} |v_{A,i}\omega_i|} \tag{8}$$

where $v_{A,i}$ is the net stoichiometric coefficient of species A within reaction i, ω_i is the net production rate of reaction i, and $\delta_{B,i}$ is the Dirac delta function. This equal 1 if the i^{th} elementary reaction is involved with species B and 0 if others.

The DRGEP relies on the fact that the influence of species B on the production and consumption rate of species A, no matter whether the r_{AB} is strong or weak, is given by Eq. (9).

$$r_{AB}^{DRGEP} = \frac{\left|\sum_{i=1}^{N_r} v_{A,i}\omega_i\delta_{B,i}\right|}{max(P_A, C_A)} \tag{9}$$

where $P_A = \sum_{i=1}^{N_r} \max(0, v_{A,i}\omega_i)$ and $C_A = \sum_{i=1}^{N_r} \max(0, -v_{A,i}\omega_i)$ are respectively the production rate and consumption rate of species A. The PFA pays attention to the production and consumption flux instead of the species interaction. The production, P_A, and consumption flux, C_A, will evaluate the interaction between two species and identify the reaction paths ways. The production and consumption flux are related to species B are expressed by Eq. (10) and Eq. (11).

$$P_{AB} = \sum_{i=1}^{N_r} \max(0, v_{A,i}\omega_i\delta_{B,i}) \tag{10}$$

$$C_{AB} = \sum_{i=1}^{N_r} \max(0, -v_{A,i}\omega_i\delta_{B,i}) \tag{11}$$

Then the r_{AB} of P_{AB} and C_{AB} are given by Eq. (12) and Eq. (13), respectively.

$$r_{AB}^{P} = \frac{P_{AB}}{max(P_A, C_A)} \tag{12}$$

$$r_{AB}^{C} = \frac{C_{AB}}{max(P_A, C_A)} \tag{13}$$

The search-initiating species are automatically selected by the progress equivalent ratio for ϕ, and ϕ_h (subscript h for a high degree of hydrocarbon fuel) in the DRGEP following combustion status, called DAC, and given by Eq. (14) and Eq. (15), respectively.

$$\phi = \frac{(2-z')\sum_{j=1,N_s}^{S_{j\neq CO_2}} Y_{S_j}N_{C,S_j} + \frac{1}{2}\sum_{j=1,N_s}^{S_{j\neq H_2O}} Y_{S_j}N_{H,S_j}}{\sum_{j=1,N_s}^{S_{j\neq CO_2,H_2O}} Y_{S_j}N_{O,S_j} - z'\sum_{j=1,N_s}^{S_{j\neq CO_2}} Y_{S_j}N_{C,S_j}} \tag{14}$$

$$\phi_h = \frac{2\sum_{j=1,N_s}^{N_{c,S_j\geq 3}} Y_{S_j}N_{C,S_j} + \frac{1}{2}\sum_{j=1,N_s}^{N_{c,S_j\geq 3}} Y_{S_j}N_{H,S_j}}{\sum_{j=1,N_s}^{N_{c,S_j\geq 3}} Y_{S_j}N_{O,S_j} + 2Y_{O_2}} \tag{15}$$

where Y_{S_j} is the mass fraction of species S_j, N_{C,S_j}, N_{H,S_j} and N_{O,S_j} is the number of atoms C, H and O in species S_j, z' is the proportion of fuel oxygen to fuel carbon (equal to zero if there is only hydrocarbon fuel without oxygen) and ϕ_h is used to consider the high degree of hydrocarbon fuel which oxygen is only considered as an oxidiser.

The reduction based on atomic consideration is called EFA. The species was taken into consideration as a source or sink species that plays a major part in the overall element flux. It is given by Eq. (16) and Eq. (17).

$$\dot{a}_{AB,i} = \left(|\omega_{fi}| + |\omega_{bi}|\right)\frac{N_{a,A}N_{a,B}}{N_{a,i}} \tag{16}$$

$$\dot{a}_{AB} = \sum_{i=1}^{N_r} \dot{a}_{AB,i}\,\delta_{AB,i} \tag{17}$$

where $\dot{a}_{AB,i}$ and $\dot{a}_{AB}$ represents element flux of atom a between species $A-B$ of reaction i and total flux, respectively. $|\omega_{fi}| + |\omega_{bi}|$ is the net production rate of reaction i, $N_{a,A}$ and $N_{a,B}$ are the numbers of atoms a in species A and B, respectively and $N_{a,i}$ is the total number of atoms a in reaction i.

Partially Premixed Flame Modelling

Following the previous work of Irandoost et al. [28], the Mach-Zehnder optical technique had used to study the axisymmetric partially premixed flame. A co-annular burner with an inner diameter of 10.6 mm and outer diameters of

38 mm operated in an open environment under the pressure and temperature of 87 kPa and 297 K, respectively. A primary flow of 99% purity of methane (CH4) mixed with pure air and secondary airflow jetted from the inner and outer tube. The experiment had focused on where the peak centerline temperature occurred. It was defined as the thermal flame height (HT) that their primary focus was on the influence of equivalent ratio and Reynolds number variation to such HT. The partially premixed flame shows with a schematic diagram in Figure 2(a).

The variation of equivalent ratio and Reynolds number were out of scope to model the partially premixed flame of experimental work. Only an equivalent ratio would assess the different reduced mechanism methods inside the TDAC framework with a constant flow rate. Consequently, the space above the burner, a diameter of 38 mm and height of 100 mm, was confined for the 2-D axisymmetric domain, which was enough to capture all the flame appearance. Figure 2(b) and 2(c) show this CFD domain and cell structure of its, respectively. All values were specified model defined according to the experiment. An inlet fuel face held a constant velocity of 0.44 m s^{-1} with the mass fraction of 0.075, 0.21275, and 0.71225 for CH4, O2, and N2, respectively. An inlet air face corresponding to secondary airflow had specified a velocity of 0.2 m s^{-1} with the mass fractions of 0.23 and 0.77 for O_2 and N_2, respectively. The wall was a no-slip condition to account for the burner rim effect. The sides and outlet faces were pressure outlet condition. The front and back faces were the wedge conditions. Initial pressure and temperature inside the cells were 87 kPa and 297 K, respectively. To be active in the chemical reaction, the small area above the burner was set at a high temperature of 1500 K. This temperature would achieve by assumption, which was enough to ignite the combustion and did not affect the simulation results. The buoyancy was incorporated in the combustion model for the driving force in the plume due to density variations. The cell structure would perform by OpenFOAM's utility called BlockMesh. The cell refinement would also carry out in the region of flame appearance following experimental results. The non-uniform cell grading of 1/2, 0.5/1, 0.25/0.5, 0.125/0.25 and 0.0625/0.125 mm (finest/coarsest) were used to perform the cell independence. It resulted that the last three cases could represent an obvious flame with no irregularity of the thermal flame height (HT). Therefore, a grid size grading of 0.25/0.5 had defined in this study. The 2nd order scheme would use in the spatial discretisation, in which the 1st order of implicit scheme had discretised a time-dependent term. The PISO coupled with SIMPLE algorithms, called PIMPLE, was used here by assigning 1 and 3 loops for inner PISO and outer SIMPLE iteration, respectively. The Courant number was 0.2 to guarantee computational stability. A central processing unit with 3.6 GHz of Intel Core i7-7700 with Quad-Core and 8 GB of RAM had used to compute all the flame models.

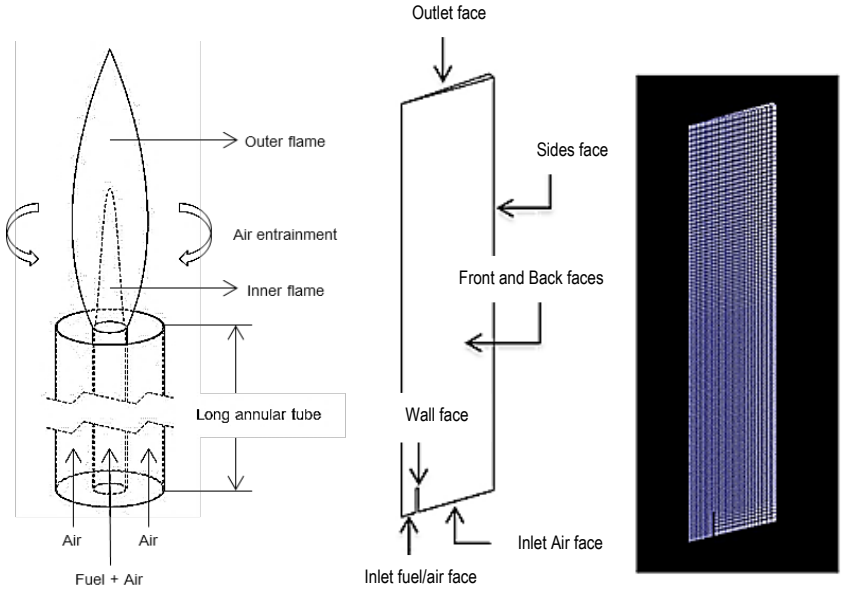

(a) (b) (c)

Figure 2. (a) The partially premixed flame flow through a co-annular burner, (b) boundary conditions, and (c) cell structure of the CFD domain.

RESULTS AND DISCUSSION

The partially premixed laminar flame models consisted of (i) the flame model without TDAC for the computational facilitation, (ii) the flame model with the ISAT (performing TDAC without mechanism reduction), and (iii) five flame models with TDAC by the five different options of reduced mechanism methods. These options comprised the DRG, DRGEP, DAC, PFA, and EFA. Therefore, a total of seven models were built to study. All the flame models except TDAC with DRGEP could reach the final desirable time step and accomplish satisfactory results. Unfortunately, the flame modelled by TDAC with DRGEP reduction could combust at the first step but blow off in the following steps. Some immediate radicals or species affecting essential reaction steps in the chain propagating and chain branching might be

eliminated by DRGEP fortuitously. These led to insufficient species or radicals that could not sustain the continuous flame. Therefore, six models would examine. All transient flame results reached a stable propensity at least 0.8 seconds approximately. For ensuring a steady state, the results would collect at 5 seconds. Figure 3 depicts the mass fraction of CH4, O2, CO2, and H2O distributions with the colour contour. They were results of the CFD model without reduced mechanisms. These results were in half conical shape. The mass fraction of CH4 and O2 existed as to their initial composition inside and disappeared outside the conical shape. This consistency implied that was no consumption of reactants (CH4 and O2) inside and the production of the product (CO2 and H2O) outside.

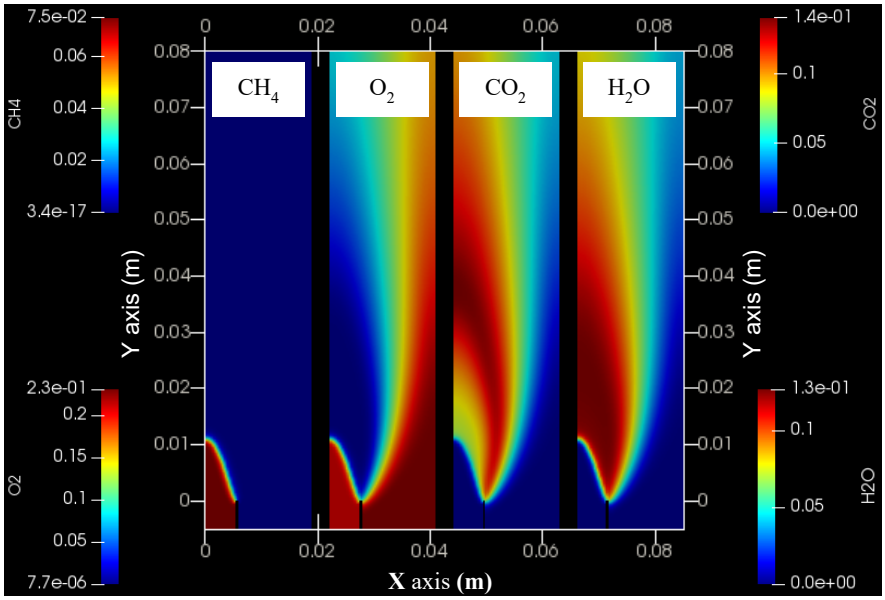

Figure 3. The distribution of mass fraction of CH_4, O_2, CO_4 and H_2O, respectively.

Figure 4 shows the parallel of actual flame by an experiment of Irandoost et al. [28] and temperature contour by CFD modelling. Figure 4(a) involves an inner and outer zone parted by a luminous flame front. The unburnt and burnt gas remained low and high temperature, respectively. An unburnt was inside in which the burnt production was across the flame front outwardly. The principle was that the chemical reactions in converting the reactants to the products along liberating the heat occurred at the finite thin layer of the flame front. A peak temperature was close to the outlying flame front in which such axial position defined thermal flame height (HT). This actual flame could be equivalent to CFD temperature contour. The cold was inside and suddenly shifted to a hot temperature outside the cone. The gradient temperature zone at the flame front is expressed in Figure 4(b). It likewise agrees with the mass fraction contour in Figure 4. The reactants and products were inside and outside of the cone.

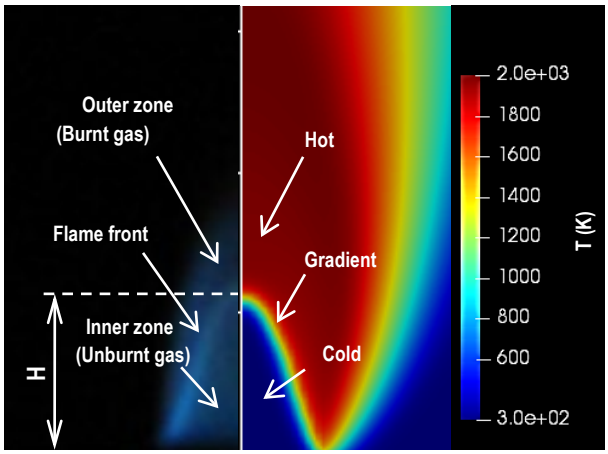

(a) (b)

Figure 4. (a) Flame height and (b) temperature contour by GRI-Mech.

It found that the heat released rate was agreed well with the experiment to identify the flame front of CFD modelling. By this definition, heat released rate (HRR) was where almost all reactions proceeded. Figure 5(a) and 5(b) illustrate the HRR contour and HRR enclosed by a white line superimposing on the temperature contour, respectively. The enclosed white line was settled at the temperature gradient zone, dividing the low- and high-temperature part. A low temperature was 297 K, similar to the unburnt reactant temperature. As it left the flame position, the burnt gas was expanded and

diluted with the surrounding air. It found that the hottest part located just above attached to the finite thin layer of the enclosed white line. Accordingly, this point matched the experimental HT for validating HT. In all six cases, HT in CFD is in good to agree with the experimental results illustrated in Figure 6. The average error was 9.87, 12.22, 11.91, 12.29, 11.42, and 11.78 for the flame model without the computational facilitation (GRI-Mech), the flame model with ISAT, the flame model with TDAC using DRG, DAC, PFA, and EFA, respectively.

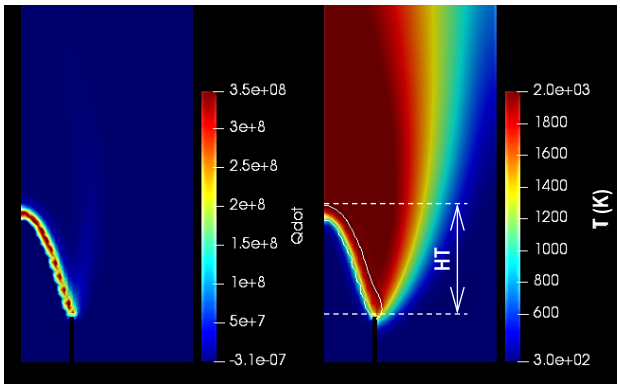

(a) (b)

Figure 5. (a) The heat released rate and (b) the confined heat released rate on temperature contour by GRI-Mech.

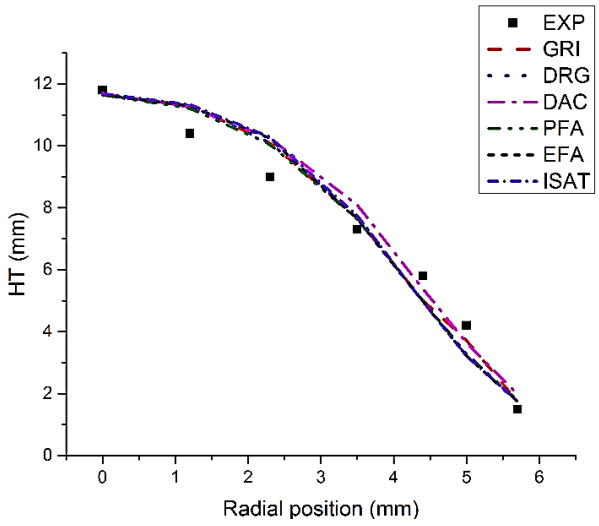

Figure 6. The comparison of thermal flame height.

Figure 7 shows the mass fraction of concentrations, temperature, and HRR are plotted along with the radial distance at 0.075 m above the burner. The dashed lines enclosed the bell curve of HRR for specifying a thin finite layer of the flame front. It comprised the preheated (PH) and reaction layers (R) which were inside. The PH, where some inside unburnt gas attached to the R layer, was heated up by thermal diffusion from the hot part. This layer was a primary mechanism for sustaining combustion. Most of the heat released from R layers used the HRR and T gradient peaks to indicate. The reactants (CH4 and O2) had consumed almost by forming products in this layer. Alternatively, the flame front could consider via a peak of OH concentration. This OH distribution inside the domain signified where the chain branching and propagating reactions proceed. It has a pair of peaks following the radius plot in Figure 8. The first peak was lower and inside the R layer that indicated the inner flame front. It was common in the rich flame that the second peak was much higher and occurred at the mixing layer, the region of a burnt product being adjacent to secondary airflow. Brunt product continued burning by supplying an oxidiser (secondary airflow). It produced a much smaller HRR compared to the inner flame front.

The flame model without computational facilitation was reasonable to be the reference case for further examining the other five models. The CFD results such as temperature, velocity, and some mass fraction contour were in good agreement with a reference case. Still, some species existed an incongruence. Figure 8 shows the colour contour of HO2, NO, and NO2. These species were difficult to measure but had a tremendous impact on combustion. The HO2 was an immediate species in propagating, branching, and recombination reaction step for sustaining and terminating combustion. The NO and NO2 were major pollutants that occurred in high-temperature combustion. Also, due to the pollution concern, it usually was the most preferred variable from combustion modelling. It should note that, from now on, the TDAC using particular methods will be called only the reduction method name. In all cases except the EFA case found the inconsistency. The fault cases could not deliver the continuous contour that also influenced other variables. As expected, the DRG and PFA gained a large negative HRR where other faults were under the prediction. These dissimilarities were unacceptable.

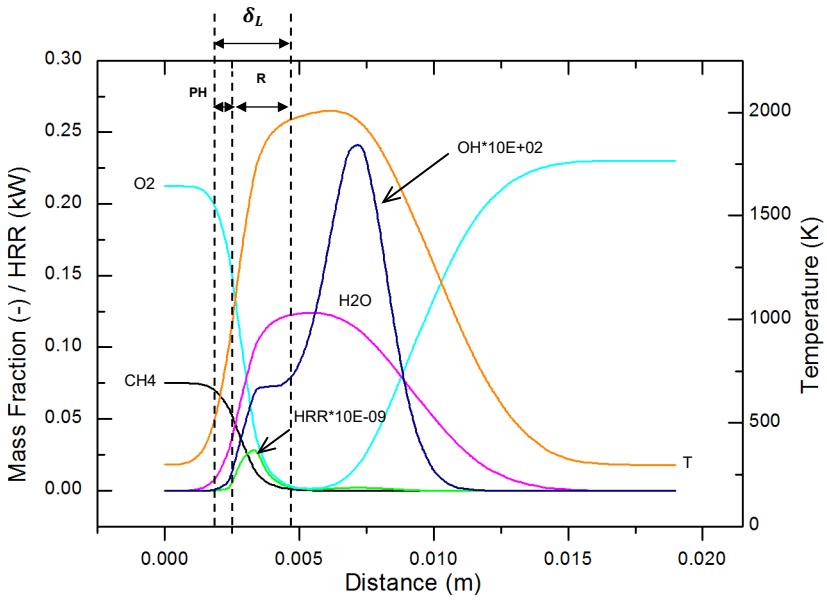

Figure 7. The radius plot of the concentration, temperature and HRR profile at 0.0075 m above the burner.

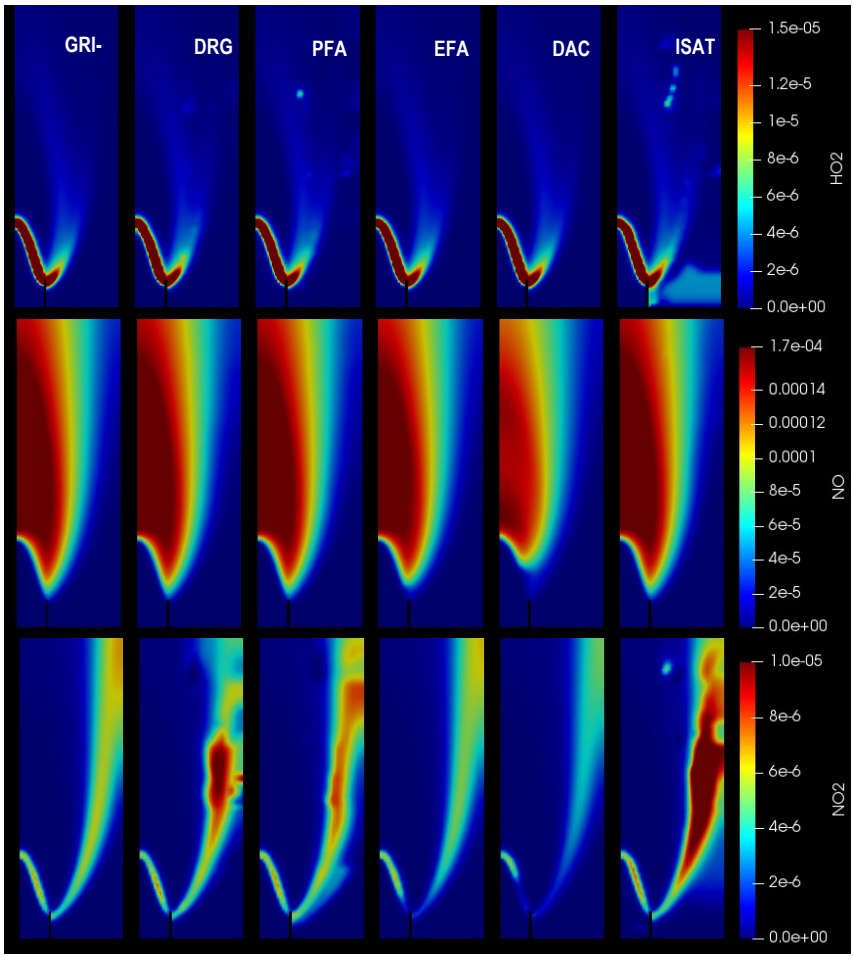

Figure. 8. The distribution of products consisting of HO2, NO and NO2, respectively.

Table 1 summarises the comparison results. The flame model without computational facilitation spent a very high computing time of 110.15 hrs. ISAT could personally shorten the computing time up to 10 times. The use of ISAT without reduction method may be uncertain, as shown in Figure 9. To be complete TDAC operation, combining ISAT with mechanism reduction method might reduce the computing time. Surprisingly, TDAC based on DRG and PFA spent more computing time than the ISAT case. Figure 9 shows the plotting of X versus runtime steps. It was rare species eliminated at the runtime for DRG and PFA in which the computation still needed the cost for the reduction method. This induced computational extravagant and uselessness. Contrarily, TDAC would be an advantage to speeding up by using TDAC based on EFA and DAC. They have reduced the computing time from using only ISAT by reducing the mechanism at runtime as authenticated by graphs in Figure 9. Even DAC was more efficient than EFA for reducing computing time

though EFA was higher accurate. It should note that the TDAC with DAC was fast even as the TDAC based on EFA could reduce the runtime active species more significantly. The reason is the algorithm in mechanism reduction to perform EFA, which added more computing tasks, was spent more time when compared to DAC. Therefore, the TDAC based on EFA was the optimal mechanism for computational investigation on the partially premixed flame. Also, it should note that the reduction methods using the production rate base (DRG, DRGEP, and DAC) and production flux base are lower performance than the element base (EFA) when adapted to the on-the-fly reduction method. In addition, DAC automatically defined the search-initiating species at the runtime, which could more accelerate the computation. Significantly, the reactants and products used to select the search-initiating species of other methods. It presumes that an appropriate selection of search-initiating species can advance TDAC based on others.

Table 1. Simulation results.

Description	Reduced mechanism					
	No TDAC	DRG	DAC	PFA	EFA	TDAC (only ISAT)
CPU time (Hrs.)	110.15	13.71	8.58	13.62	10.44	12.00
Max. temp. (K)	2076.58	2076.20	2076.31	2076.30	2076.57	2076.50
Max. heat released	3.5×10^{8}	3.5×10^{8}	3.5×10^{8}	3.5×10^{8}	3.5×10^{8}	3.5×10^{8}
Min. heat released	-3.1×10^{-7}	-1.0×10^{4}	-2.0×10^{-1}	-2.5×10^{5}	-2.0×10^{-1}	-1.5×10^{-1}
% average error by comparing HT	9.87	11.90	12.29	11.42	11.78	12.22

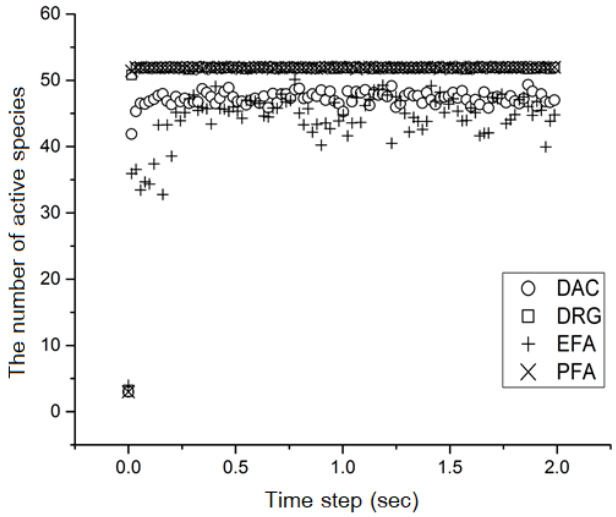

Figure 9. The number of active species vs time step of different reduction methods.

CONCLUSION

The partially premixed flame model had accomplished with an open-source CFD software based on FVM called OpenFOAM. A total of seven models, in this work, comprised one direct computing flame model and six flame models with the computer facilitation technique (TDAC), in which all employed GRI-Mech 3.0 for detailing a chemical evolution. The six of seven CFD models could reproduce the temperature, velocity, pressure, and mass fraction in which HRR proposed to capture the flame front location in the CFD result. They were in good agreement with the experimental data of Irandoost et al. [28] for HT. In the comparison, all the errors were less than 12.5%. The overall conclusion is that the efficiency of TDAC on a partially premixed flame model was satisfactory for much less computing time to 10 times compared to direct computing. Predominantly, TDAC based on EFA was the second-fastest but the most accurate option. This option can skip the time-consuming or computing cost limitation, especially on a personal computer. It is a valuable tool in designing and analysing complex combustion applications with shorter computing time and pleasant accuracy.

ACKNOWLEDGEMENT

This work was supported by The 60th Year Supreme Region of His Majesty King Bhumibol Adulyadej Scholarship, granted by the Faculty of graduate studies academic year 2016, Mahidol University.

REFERENCES

[1] R. Turns, *An introduction to combustion: Concepts and applications*, McGraw-Hill, New York, United States, 2012.
[2] W.K. Metcalfe, S.M. Burke, S.S. Ahmed, H.J. Curran, "A hierarchical and comparative kinetic modeling study of c1-c2 hydrocarbon and oxygenated fuels", *Int. J. Chem. Kinet.,* vol 45, no. 10, pp. 638-675, 2013, doi: 10.1002/kin.20802.
[3] T. Lu, and C. K. Law, "Toward accommodating realistic fuel chemistry in large-scale computations", *Prog. Energy Combust.*, vol 35, no. 2, pp. 192-215, 2009, doi: 10.1016/j.pecs.2008.10.002.

[4] R. B. Bird, W. E. Stewart, and Edwin N. Lightfoot, *Transport Phenomena,*, John Wiley & Sons, Inc., New York City, United States, 2002.
[5] E. L. Cussler, *Diffusion: Mass transfer in fluid systems*, Cambridge University Press, Cambridge, United Kingdom, 2009.
[6] N. J. Curtis, K.E. Niemeyer, C.J. Sung, "An investigation of GPU-based stiff chemical kinetics integration methods", *Combust. Flame*, vol. 179 no. May, pp. 312-324, 2017, doi: 10.1016/j.combustflame.2017.02.005
[7] S. Xi, J. Xue, F. Wang, and X. Li, "Reduction of large-size combustion mechanisms of n-decane and n-dodecane with an improved sensitivity analysis method," *Combust. Flame*, vol 222, pp. 326–335, 2020, doi: 10.1016/j.combustflame.2020.08.052.
[8] B. W. Lung Chai *et al.*, "Complex chemical kinetic mechanism reduction for simultaneous catalytic oxidation and desulphurisation of hydrogen sulphide", *Fuel,* vol. 286 no. Febuary, 2021, doi: 10.1016/j.fuel.2020.
[9] T. Lu, and C. K. Law, "On the applicability of directed relation graphs to the reduction of reaction mechanisms", *Combust. Flame,* vol. 146 no. 3, pp. 472–483 2006, doi: 10.1016/j.combustflame.2006.04.017.
[10] P. Pepiot-Desjardins, and H. Pitsch, "An efficient error-propagation-based reduction method for large chemical kinetic mechanisms", *Combust. Flame*, vol. 154, no. July, pp. 67–81, 2008, doi: 10.1016/j.combustflame.2007.10.020.
[11] L. Tosatto, B.A. V. Bennett, and M. D.Smooke, "Comparison of different DRG-based methods for the skeletal reduction of JP-8 surrogate mechanisms", *Combust. Flame* vol. 160, no. 9, pp. 1572-1582, 2013, doi: 10.1016/j.combustflame.2013.03.024.
[12] W. Sun, Z. Chen, X. Gou, and Y. Ju, "A path flux analysis method for the reduction of detailed chemical kinetic mechanisms", *Combust. Flame*, vol. 157, no. 7, pp. 1298–1307, 2010, doi: 10.1016/j.combustflame.2010.03.006.
[13] F. Perini, J. L. Brakora, R. D. Reitz, and Giuseppe Cantore, "Development of reduced and optimised reaction mechanisms based on genetic algorithms and element flux analysis", *Combust Flame*, vol. 159, no. 1, pp. 103–119, 2012, doi: 10.1016/j.combustflame.2011.06.012.
[14] R. Fournet *et al.*,"Automatic reduction of detailed mechanisms of combustion of alkanes by chemical lumping", *Int. J. Chem. Kinet.,* vol. 32, no. 1, pp. 36-51, 2000, doi: 10.1002/(SICI)1097-4601(2000)32:1<36::AID-JCK5>3.0.CO;2-0.
[15] Alison S. Tomlin *et al.*, "Mechanism reduction for the oscillatory oxidation of hydrogen: sensitivity and quasi-steady-state analyses", *Combust. Flame*, vol. 91, pp. 107-130, 1992, doi.org/10.1016/00102209308924120.
[16] M. Rein, "The partial-equilibrium approximation in reacting flows", *Phys. Fluids,* vol. 4, pp. 873-886, 1992, doi: 10.1063/1.858267.
[17] S. H. LAM, "Using CSP to understand complex chemical kinetics", *Combust. Sci. Technol.,* vol. 89, pp. 375-404, 1993, doi.org/10.1080/0010-2180(92)90094-6.
[18] U.Maas and S. B. Pope, "Simplifying chemical kinetics: Intrinsic low-dimensional manifolds in composition space", *Combust. Flame*, vol. 88, no. 3, pp. 239-264, 1992, doi: 10.1016/0010-2180(92)90034-M.
[19] L. E. Whitehouse, A. S. Tomlin, M. J. Pilling. "Systematic reduction of complex tropospheric chemical mechanisms, Part I: sensitivity and time-scale analyses". *Atmos. Chem. Phys., European Geosciences Union*, vol. 4, no. 7, pp. 2025-2056, 2004, doi: 10.5194/acp-4-2025-2004.
[20] J. Y. Chen, J. A. Blasco, N. Fueyo, and C. Dopazo, "An economical strategy for storage of chemical kinetics: Fitting in situ adaptive tabulation with artificial neural networks", *Proc. Combust. Inst.,* vol. 28, no. 1, pp. 115–121, 2000, doi: 10.1016/S0082-0784(00)80202-7.
[21] F. Contino, H. Jeanmart, T. Lucchini, and G. D'Errico, "Coupling of in situ adaptive tabulation and dynamic adaptive chemistry: An effective method for solving combustion in engine simulations", *Proc Combust Inst.,* vol 33, no. 2, pp. 3057–3064, 2011, doi: 10.1016/S0082-0784(00)80202-7.
[22] F. Contino *et al.*, "Experimental and numerical analysis of nitric oxide effect on the ignition of iso-octane in a single cylinder HCCI engine", *Combust. Flame*, vol. 160, no. 8, pp. 1476–1483, 2013, doi: 10.1016/j.combustflame.2013.02.028.
[23] Francesco Contino, *et al.*, "CFD simulations using the TDAC method to model iso-octane combustion for a large range of ozone seeding and temperature conditions in a single cylinder HCCI engine", *Fuel*, vol. 137, no. 1, pp. 179–184, 2014, doi: 10.1016/j.fuel.2014.07.084.
[24] J. An *et al.*, "Dynamic adaptive chemistry with mechanisms tabulation and in situ adaptive tabulation (ISAT) for computationally efficient modeling of turbulent combustion", *Combust flame*, vol. 206, pp. 467–475, 2019, doi: 10.1016/j.combustflame.2019.05.016.
[25] H. G. Weller, G. Tabor, H. Jasak, and C. Fureby, "A tensorial approach to computational continuum mechanics using object-oriented techniques", *Comput. Phys.,* vol. 12, no. 6, 1998, doi: 10.1063/1.168744.
[26] C. Suvanjumrat, "Implementation and validation of OpenFOAM for thermal convection of flow," *Engineering Journal*, vol. 21, no. 5, pp. 225-241, 2017, doi: 10.4186/ej.2017.21.5.225.
[27] G. P. Smith *et al.*, [Online] Available: http://www.me.berkeley.edu/gri_mech/ [Accessed March 1, 2021].
[28] M. S. Irandoost, M. Ashjaee, M. H. Askari, and S. Ahmadi, "Temperature measurement of axisymmetric partially premixed methane/air flame in a co-annular burner using Mach–Zehnder interferometry", *Opt. Lasers Eng.*, vol. 74, no. , pp. 94–102, 2015, doi: 10.1016/j.optlaseng.2015.05.013.